energy&fuels

pubs.acs.org/EF

Article

Elucidation of Structure and Physical Properties of Pyrolytic Sugar Oligomers Derived from Cellulose Depolymerization/Dehydration Reactions: A Density Functional Theory Study

Published as part of the Energy & Fuels virtual special issue "Highlighting Contributions from Our Editorial Board Members (2023)".

Melba Domes Denson, Evan Terrell, Pavlo Kostetskyy, Mariefel Olarte, Linda Broadbelt, and Manuel Garcia-Perez*

Cite This: *Energy Fuels* 2023, 37, 7834–7847

Read Online

ACCESS | Metrics & More | Article Recommendations | Supporting Information

ABSTRACT: Fast pyrolysis of lignocellulosic materials is a promising research area to produce renewable fuels and chemicals. Dehydration is known to be among the most important reaction families during cellulose pyrolysis; water is the most important product. Together with water, dehydration reactions also form a range of poorly known oligomer species of varying molecular sizes, often collected as part of the bio-oil water-soluble (WS) fraction. In this work, we used electronic structure calculations to evaluate the relative thermodynamic stabilities of several oligomer species from cellulose depolymerization intermediates undergoing three consecutive dehydration events. A library of the thermodynamically favored candidate molecular structures was compiled. Results revealed that most of the water molecules are eliminated from the non-reducing end, forming thermodynamically more stable conjugated compounds. This is consistent with results reported in literature where dehydration reactions occur preferably at the non-reducing ends of oligomers. The theoretical Fourier-Transform Infrared Spectroscopy and NMR spectra of these proposed sugar oligomers conform qualitatively to the experimental result of pyrolytic sugars. Understanding their chemical structure could help to develop rational strategies to mitigate coke formation as sugars are often blamed to cause coke formation during bio-oil refining. The estimated physical–chemical properties (boiling point, melting point, Gibbs free energy of formation, enthalpy of formation, and solubility parameters among others) are also fundamental to conducting first-principles engineering calculations to design and analyze new pyrolysis reactors and bio-oil up-grading units.

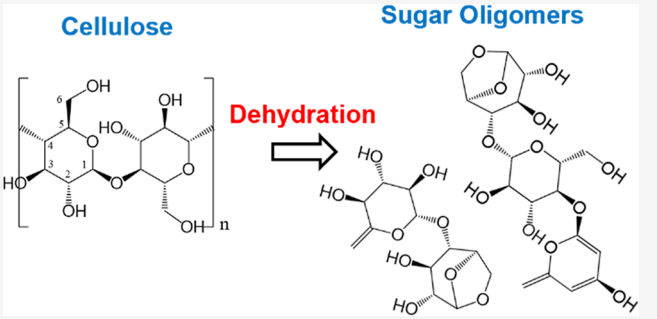

1. INTRODUCTION

Continued global population growth, industrialization, environmental concerns, and depletion of fossil fuel reserves demand the diversification of our energy portfolio.[1−3] Lignocellulosic biomass, abundant, inexpensive, and non-competing for food resources, is a renewable source of C to produce fuels and chemicals. Cellulose is the most abundant biomolecule synthesized by photosynthesis.[4−6] It is composed of repeating D-glucose units connected by β-1-4 glycosidic bonds.[7,8] Cellulose can be decomposed into various chemical species through different methods including thermal decomposition (e.g., fast pyrolysis).[3]

Fast pyrolysis is a promising conversion method where biomass is subjected to moderately high temperatures (673 to 873 K) without oxygen.[9,10] Several chemical transformations occur in a complex network of chemical reactions as the cellulose polymer chain breaks apart. During fast pyrolysis, dehydration reactions result in water formation and poorly known anhydrous sugars.[11−13] This is coherent with the experimental results obtained by Stankovikj et al.[14] Terrell and Garcia-Perez[15] compared experimental results with hypothetical pathways and assigned tentative chemical structures to the dehydrated oligomers observed using Fourier transform ion cyclotron resonance mass spectrometry (FT-ICR MS).

While experimental results give significant insights regarding molecular mass and elemental composition of anhydrosugars, complementing these results with first-principles calculations could generate new information on the reaction mechanisms

Received: February 25, 2023
Revised: April 20, 2023
Published: May 10, 2023

https://doi.org/10.1021/acs.energyfuels.3c00641
Energy Fuels 2023, 37, 7834–7847

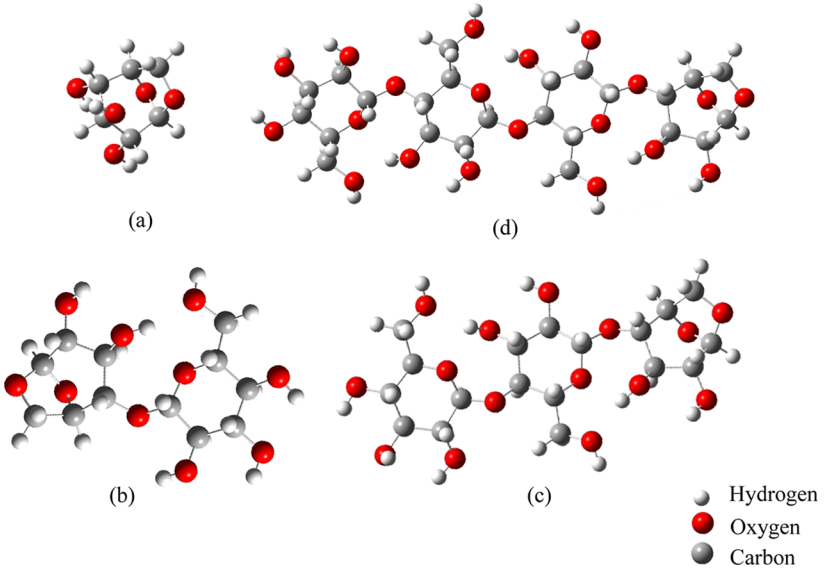

Figure 1. Optimized structures of the model compounds: (a) levoglucosan, (b) cellobiosan, (c) cellotriosan, and (d) celloquatrosan.

and molecular structure of pyrolysis products. Hu et al.[16] and Kostetskyy and Broadbelt[17] discussed the recent developments of using electronic structure calculations to assess the mechanisms of biomass pyrolysis via quantum chemistry (QC). They concluded that the use of QC modeling provides deep insights to obtain a whole image of the complex biomass pyrolysis chemistry (for both reaction mechanisms and product structures), which are experimentally difficult to grasp. Nimlos et al.[18,19] used electronic structure calculations to study the dehydration mechanism of alcohols and glycerol and concluded that their work could be extended for carbohydrates. Hosoya and Sakaki[20] investigated the formation of levoglucosan using dimer and hexamer oligomeric carbohydrate models to represent the native cellulose. Results of their study showed that dimer degradation occurs by means of a concerted mechanism. The one-chain hexamer model showed no formation of levoglucosan; instead, depolymerization occurred. Two-chain models with interchain H bonds clearly showed the formation of levoglucosan, and three-chain models indicated selective degradation on the crystalline surface. Easton et al.[13] studied four water loss mechanisms of glucose and cellobiose during cellulose-fast pyrolysis. Their results showed that aldol condensation has the lowest free-energy barrier, which is consistent with cellobiose, and therefore could be applicable to glucooligosaccharides with a higher degree of polymerization. Zhang et al.[21] modeled the mechanism of levoglucosan thermal decomposition during pyrolysis employing direct C−C bond breaking, C−O bond breaking, and 1,2-dehydration and found that the latter is the most favorable pathway, removing the hydroxyl group from C2 and a hydrogen atom from C3. These computational works contribute toward a comprehensive understanding of the elementary reaction mechanisms of cellulose and could pave ways to further study the heavy unknown oligomeric fractions of the bio-oil.

The presence of anhydrosugar oligomers in bio-oil formed during cellulose pyrolysis was discussed by Mamleev et al.[22] The study by Pecha et al.[23] on the fast pyrolysis of hybrid poplar between 0.4 and 100 kPa revealed the effect of pressure on the formation of bio-oil anhydrosugars. Stankovikj et al.[14] also confirmed the presence of highly dehydrated oligomeric sugars in fast pyrolysis from cellulose using FT-ICR/MS. The mechanistic modeling of fast pyrolysis of neat glucose-based carbohydrates by Zhou et al.[24] predicted the formation of anhydrosugar products. These pyrolytic sugars are becoming an important field of research because they can be converted easily to platform chemicals such as furanics.[25,26]

The thermodynamic and physical properties of these compounds, such as boiling point, critical temperature, and pressure, enthalpy of formation and vaporization, enthalpy of fusion, standard Gibbs free energy of formation, solubility parameters, and so forth, are fundamental to understanding their behavior in the mixtures and needed for the design of extraction/conversion, separation, and upgrading processes.[27] In the absence of experimental data due to cost or time constraint, methods for estimation of thermophysical properties of compounds must rely on theoretical tools, such as quantum mechanics, empirical correlations, and group additivity-based methods. Estimation methods usually apply the concepts of quantitative structure−property relationships (QSPRs) and quantitative property−property relationships (QPPRs), varying by the type of input data. QSPR methods require only knowledge of the molecular structures of the compound to estimate their physical properties while QPPR uses thermodynamic data.[28] The group contribution method (GCM), a special case of QSPR approach, is a simple, quick, and extensively used technique that relies on the additivity principle of individual group contributions.[29] The best known GCM include the first-order approximations by Joback,[30] Joback & Reid et al.,[60] Lydersen et al.,[55] and Stein and Brown.[31] These authors developed mathematical models employing multiple linear regression techniques to determine the group contributions from each fragment.

In this work, we aim to elucidate and propose potential structures of the oligomeric sugar compounds found in bio-oil through electronic structure calculations and then estimate their physical and thermodynamic properties. Dehydrated sugars, particularly levoglucosan, being the main product of fast cellulose pyrolysis,[32,33] and its oligomeric units (up to tetra-state), linked by 1,4-β-glycosidic bonds, were used as the starting model compounds. An in-depth understanding of these compounds' structure will contribute to developing and

https://doi.org/10.1021/acs.energyfuels.3c00641
Energy Fuels 2023, 37, 7834−7847

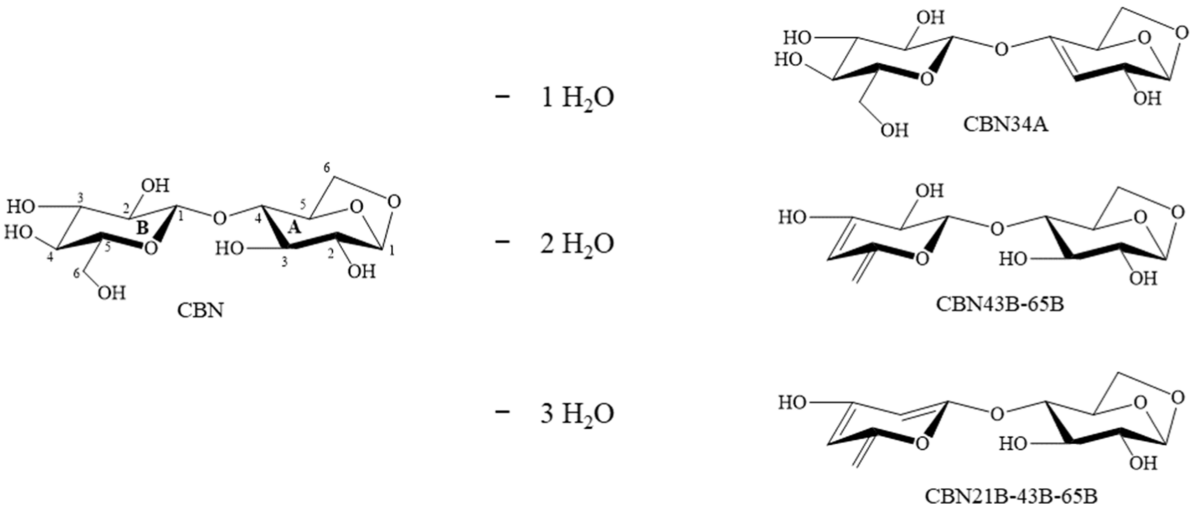

Figure 2. Sequential dehydration and numbering scheme for CBN. CBN stands for cellobiosan, A for the LG-end, and *B* for the NR-end (in the case of cellotriosan, *B* stands for the internal unit and *C* for the NR-end; the same pattern was followed for celloquatrosan).

advancing biomass pyrolysis techniques and product upgrading strategies, especially hydrotreatment where coke formation is believed to be caused by the presence of sugar oligomers.

2. METHODOLOGY

2.1. Computational Details. The model compounds, shown in Figure 1, were subjected to dehydration reaction by means of the Maccoll elimination mechanism (otherwise known as 1−2 dehydration), where a C−O bond is broken with a concerted proton loss from a beta position, moving to the oxygen atom to form a CC (double bond) and eliminate water.[13] Sequential dehydrations (up to 3×) of these model compounds were completed in the gas phase with and typical fast pyrolysis temperature of 773.15 K and pressure of 1 atm. All possible pathway permutations eliminating water around the model molecules were investigated. For example, the double dehydration of the cellobiosan water molecule is eliminated from the levoglucosan-end (LG-end) and the second, from the nonreducing-end (NR-end). Another possible route is eliminating both water molecules from the same ring structure. It should be noted that the kinetics of these dehydration events was not considered; only the relative thermodynamics stabilities of the different isomers were studied as the study focused more on the structure of the final product and not the rate of reaction. The most thermodynamically stable structure has the minimum Gibbs free energy, and these calculated stabilities also provide information on whether the reaction is endothermic or exothermic. Though, kinetics is also a good parameter to consider for future studies.

A systematic naming convention was assigned to identify the reactants, intermediates, and products. LG stands for levoglucosan, CBN for cellobiosan, CTN for cellotriosan, and CQN for celloquatrosan. For example, in CBN34A, CBN stands for cellobiosan as the name of the molecule under study; A refers to ring 1 being the LG-end, the first number "3" specifies the carbon position where the hydroxyl group is removed, and the second number "4" identifies the hydrogen atom being eliminated. This numbering convention is illustrated in Figure 2.

Geometry optimization and frequency calculations of all reactants, intermediates, and products were performed using the Gaussian 16 (Revision C.01) electronic structure code.[61] Errors associated with the calculations of structure and electronic properties include the inaccurate description of electron correlation, anharmonicity, and the solvation of the Schrodinger equation[34] but can be corrected by using scaling factors to obtain a more accurate result. The choice of correct functionals and basis set are then important to consider. The M05-2X hybrid functional[35] is recommended for carbohydrates, but we employed the newer version, M06-2X[36] and 6-311++G(d,p) basis set for the O, C, and H atoms. Each converged geometry was verified with vibrational frequency calculations for all structures. A scaling factor of 0.9567 was used for the calculated vibrational frequencies, based on the work of Ünal et al.[34] The change in free energy for subsequent dehydration events of the model compounds was calculated according to eq 1, where $E_{\mathrm{deh,H_2O}}$ corresponds to the

$$E_{\mathrm{deh,H_2O}} - E_{\mathrm{carb}} \tag{1}$$

energy of the dehydrated carbohydrate−H_2O complex and E_{carb} is the energy of the reacting carbohydrate. The structure of the reactant carbohydrate used for each subsequent dehydration event was then that of a carbohydrate-only, assuming desorption of water.

With the optimized and most stable product structures being identified, the theoretical nuclear magnetic resonance (both ^{1}H NMR and ^{13}C NMR) spectra were calculated using the M06-2X hybrid functional, 6-311+G(d,p) basis set, and the gauge-independent atomic orbital method. It is necessary to understand that nuclear magnetic resonance (NMR) spectra strongly depend on the molecular structure since they are constantly in motion. Thus, we make sure to use the lowest energy structure of the molecule of interest to generate the NMR spectra of the stable products. Also, NMR spectra of the typically used reference molecule, deuterated dimethyl sulfoxide (DMSO), was calculated, and the shielding value was subtracted from the spectrum of the stable products to obtain the relative shifts. Theoretical results may slightly vary for different functionals and basis sets and the type of reference molecule employed for NMR calculations.

2.2. Validation of Simulations. Selected model compounds, namely, D-glucose (Dextrose) anhydrous (≥99%, Thermo Scientific Chemicals), D(+)-mannose (≥99%, Sigma-

https://doi.org/10.1021/acs.energyfuels.3c00641
Energy Fuels 2023, 37, 7834−7847

Aldrich), and levoglucosan (99.3%, AK Scientific, Inc.), were subjected to both experimental and theoretical Fourier-Transform Infrared Spectroscopy (FTIR) and NMR analyses to assess the validity of the modeling results. Experimental FTIR results were recorded in the solid phase using a Shimadzu IRPrestige 21 spectrometer equipped with a MIRacle single reflection ATR Ge probe. Enough samples were applied to cover the crystal window for measurement. Spectra were acquired at 600−4000 cm^{-1} and a resolution of 4 cm^{-1}, but only the fingerprint region is shown in Figure 3.

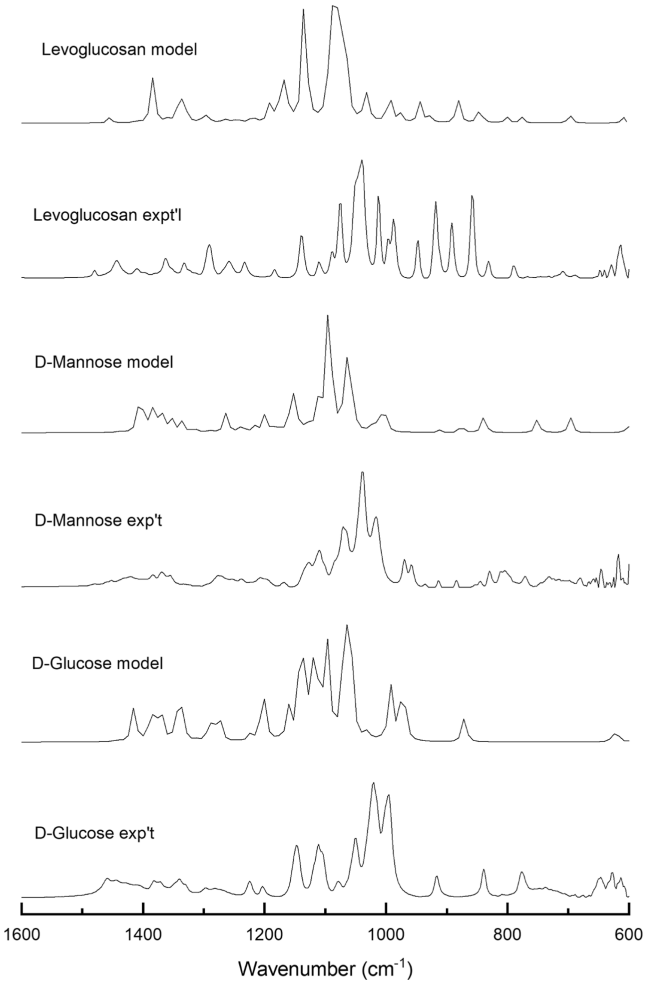

Figure 3. Comparison between experimental and modeled FTIR spectra of selected sugars.

Modeling results were calculated in the gas phase employing the same method described earlier. Comparable results were observed between the experimental and modeling for the model compounds, as shown in Figure 3. The sum of areas under the bands from 950 to 1200 cm^{-1} wavenumbers are assigned to C−O stretch vibrations of alcohols.[37,38] The calculated spectra are harmonic frequencies and thus shifted to a higher energy than the experimental spectra.[39]

Experimental ^{13}C NMR and ^{1}H NMR of the whole sugar were also obtained and compared with modeling yields. Pyrolytic sugars were separated from the whole bio-oil (BTG, The Netherlands) by means of cold-water precipitation,[40] followed by column chromatography (Sepabeads SP207)[41] to separate the sugars from phenols and finally rotary evaporation to concentrate the sugars. The ^{13}C NMR spectra were acquired on a Bruker 500 Neo spectrometer equipped with a 5 mm Prodigy broadband cryoprobe with *Z*-axis gradients. An amount of 30 mg each of the selected model compounds was dissolved in 0.7 ml of DMSO-d_6 (99.9%, Cambridge Isotope Laboratories, Inc.). The ^{13}C NMR spectra were acquired at 125.77 MHz with a 90° pulse angle (10.0 ms), 1.08 s acquisition time, relaxation delay d1 of 2 s, and inverse-gated ^{1}H composite pulse decoupling using 4000 scans, a spectral width of 30,120.5 Hz and 32,768 points. The FID was apodized with 8 Hz exponential line broadening for the model compounds. MestreNova 14.3.0 software was used for post-processing spectra. Results (Figure 4) showed a good

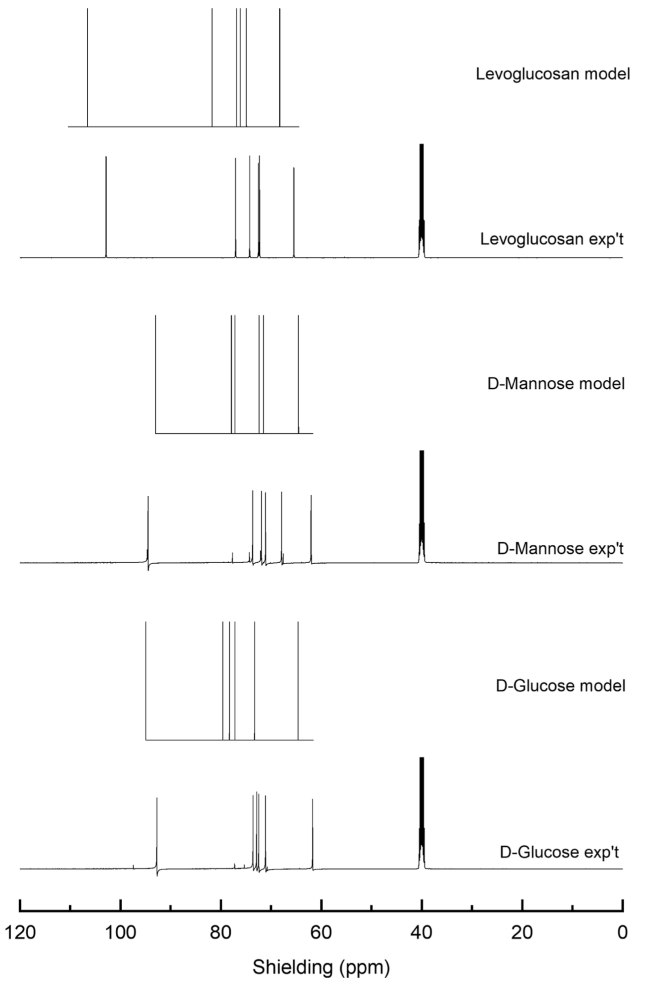

Figure 4. Comparison between experimental and modeled ^{13}C NMR spectra of selected sugars (solvent peak: DMSO = 39.7 ppm).

agreement between the experimental and modeling yield except for the shifting at 39.7 ppm in experimental results, which is attributed to the solvent used (DMSO-d_6). The integration region between 60 and 80 ppm belongs to the aliphatic C−O associated with hydroxyl groups of the sugar compounds.[12]

2.3. Estimation of Properties of the Proposed Structures. QPPRs and GCM methods were applied to estimate the important physical and thermodynamic properties of the proposed oligomeric sugar structures. The complete equations and procedures are found elsewhere.[42] Briefly, the number frequency of each group that constitutes the pure compound or mixture was summed up and then multiplied by

https://doi.org/10.1021/acs.energyfuels.3c00641
Energy Fuels 2023, 37, 7834−7847

Table 1. Most Thermodynamically Stable Structures of the Dehydrated Sugars[a]

reaction label	product structure	molecular formula	molar mass (g/mol)	ΔG_{rxn} (kJ/mol)	ΔH_{rxn} (kJ/mol)	ΔS_{rxn} (J/mol K)
LG23		$C_6H_8O_4$	144.13	-88.63	38.43	164.0
LG32-45B	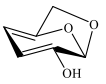	$C_6H_6O_3$	126.11	18.12	272.67	329.0
CBN34A	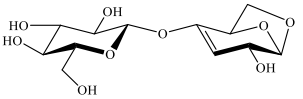	$C_{12}H_{18}O_9$	306.27	-76.85	59.27	175.0
CBN43B-65B	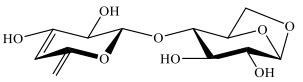	$C_{12}H_{16}O_8$	288.25	-171.67	88.63	337.0
CBN21B-43B-65B	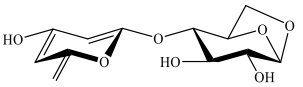	$C_{12}H_{14}O_7$	270.07	-257.53	137.70	510.0
CTN34A	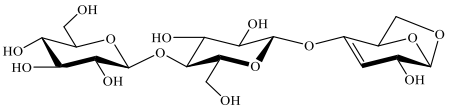	$C_{18}H_{28}O_{14}$	468.41	-82.95	53.25	180.0
CTN43C-65C	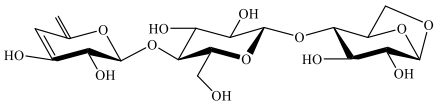	$C_{18}H_{26}O_{13}$	450.39	-177.84	79.97	333.0
CTN21C-43C-65C	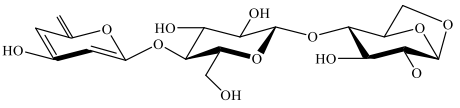	$C_{18}H_{24}O_{12}$	432.13	-269.79	129.25	516.0
CQN34A	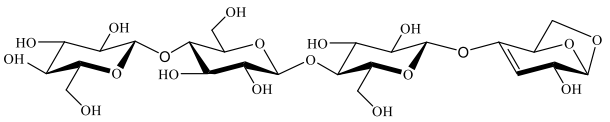	$C_{24}H_{38}O_{19}$	630.20	-79.07	53.91	172.0
CQN43D-65D	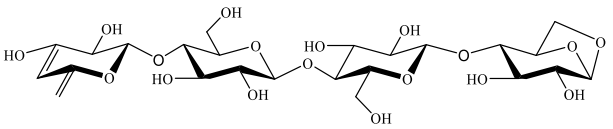	$C_{24}H_{36}O_{18}$	612.19	-164.53	93.48	334.0
CQN21D-43D-65D	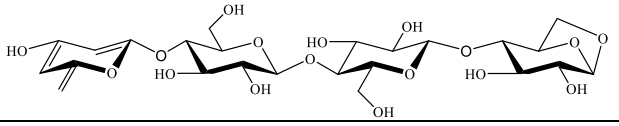	$C_{24}H_{34}O_{17}$	594.18	-255.00	131.13	499.0

[a]Note: Water is also a product but is not shown here.

their corresponding group contribution terms. Among the discrepancies associated with these methods are reliability due to over simplicity of the molecular structures, which makes isomers indistinguishable, size of model compounds, and the need of experimental data, which may not be always available.[27] Therefore, the second-order group contributions were built on the first-order groups to at least capture more information on the molecular structure of compounds like the fine differences among isomers and conjugate forms.[27,43] In this work, the first-group contributions were employed for reasons of model simplification and user friendliness. Fonts et al.[42] and Manrique et al.[44] used these same methods to estimate the physical and thermodynamic properties of bio-oil compounds derived from the fast pyrolysis of lignocellulosic compounds.

The parameters evaluated in this study are the critical properties, ideal gas properties, and condensed gas properties. The critical properties such as critical temperature (T_c), critical volume (V_c), and critical pressure (P_c) were estimated employing the methods of Joback[30] and Lydersen et al.;[55] the enthalpy of vaporization via the methods of Joback,[30] Riedel,[57] and QPPR methods; the enthalpy of fusion by the Joback[30] method; the normal boiling point by Joback[30] and Stein and Brown[31] methods; and the normal melting point by Joback and Reid[60] and Pérez Ponce et al.[58] methods. The thermodynamic properties estimated using DFT were heat

https://doi.org/10.1021/acs.energyfuels.3c00641
Energy Fuels 2023, 37, 7834−7847

capacity, standard Gibbs free energy, change in enthalpy, and change in entropy. The methods of Joback and Harrison and Seaton[45] were also employed for gas heat capacity estimation. Finally, the condensed phase properties considered were liquid heat capacity obtained by the Chueh and Swanson[59] method; the solid heat capacity obtained by the Hurst and Keith Harrison[46] method; the liquid enthalpy of formation of individual compounds via the QPPR approach; and the Hansen solubility parameters obtained by the Stefanis and Panayiotou[47] method.

3. RESULTS AND DISCUSSION

3.1. Stable Structures of the Anhydrosugars. Table 1 shows the most thermodynamically stable molecular structures identified as the likely constituents of the dehydrated anhydro-oligo-sugars. The selection of the most stable structure was based on the conformer that gives the minimum Gibbs free energy. Note that although water is a product, it was not shown in the table. Dehydration of depolymerized cellulose oligomers is one of the main pyrolytic chemical transformations. A library of product structures, assessing all possible permutations of three dehydration events, and their corresponding stability is shown as Supporting Information (Tables S1−S11).

3.1.1. Monomer. There are six possible routes by which water can be removed from a levoglucosan molecule (see Supporting Information Table S1). The result shows that pathway LG23 gave the most thermodynamically stable dehydration route with the lowest Gibbs free energy (ΔG) change of −88.6 kJ/mol. This means that the loss of a hydroxyl group from carbon 2 and hydrogen from carbon 3 is the most thermodynamically stable product. This finding is consistent with the result of Zhang et al.,[21] where they reported that the dehydration reaction is most favorable when H is removed from carbon 3 and the hydroxyl group is removed from carbon 2. On the one hand, LG21 and LG45 are less stable due to the presence of the bridged ring. Further, the changes in enthalpy (ΔH) and entropy (ΔS) of the most thermodynamically favored structure are 38.4 kJ/mol and 164 J/mol K, respectively.

For the double dehydration of levoglucosan, a total of 11 possible pathways were investigated (see Supporting Information Table S2). Results show that the double dehydration of levoglucosan is a non-spontaneous reaction as depicted by the positive value of the ΔG_{rxn}. This result is coherent with experimental results, wherein we only observe levoglucosenone products, and no other dehydrated product of levoglucosenone. Also, since levoglucosan is very volatile, it significantly vaporizes upon formation,[24,48] justifying the abundance of levoglucosan in experimental results.[12,22]

It was observed that not only water and molecules with alkene moieties are formed as products but also some alkynes. Furthermore, conjugated, isolated, and cumulated dienes are formed. However, results showed that conjugated alkenes are the most stable products. Reaction LG32A-45B, a conjugated diene, gives the most thermodynamically stable structure with Gibbs free energy change of 18.1 kJ/mol. The first water is eliminated from the LG-end at carbon 3 and carbon 2, while the second is removed at carbon 4 and 5. This result is supported by the basic knowledge on diene stability. Conjugated dienes are most stable compared to isolated and cumulated diene due to several factors like delocalization of charge through resonance and hybridization energy. Also, when comparing alkenes and alkynes, alkenes are more thermodynamically stable than alkynes. Moreover, this most stable reaction's enthalpy and entropy change accounts for 272.7 kJ/mol and 329 J/mol K, respectively. The same result was observed with the single dehydration reaction, where the dehydration routes near the bridge ring give the least favorable pathway.

3.1.2. Dimer. A total of 11 reaction pathways were examined for the single dehydration of cellobiosan (see Supporting Information Table S3). The result shows that reaction CBN34A results in the most thermodynamically stable product with a ΔG_{rxn} of −76.9 kJ/mol. This pathway involves removing the hydroxyl group from carbon 3 and hydrogen from carbon 4. Enthalpy and entropy changes were calculated to be 59.7 kJ/mol and 175 J/mol K, respectively.

The double dehydration of cellobiosan can evolve through a total of 48 reaction permutations (see Supporting Information Table S4). Results show that CBN43B-65B with a ΔG_{rxn} of −171.7 kJ/mol resulted in the most thermodynamically stable product among all the reactions. This involves the removal of two water molecules from the NR-end. The first hydroxyl group of the first water is desorbed from carbon 4 and the hydrogen atom from carbon 3. In contrast, for the second dehydration event, the hydroxyl group is eliminated from carbon six and the hydrogen atom from carbon 5. Water elimination is more facile from the NR-end relative to the LG-end due to the stability of the levoglucosan end. The same observation as in the double dehydration of the monomer is seen here, where there are formations of alkenes and a few alkynes. The most thermodynamically favorable route, which is CBN43B-65B, is a conjugated alkene. Enthalpy and entropy changes are calculated to be 88.6 kJ/mol and 337 J/mol K, respectively.

For the triple dehydration of cellobiosan, a total of 44 dehydration reactions were investigated (see Supporting Information Table S5). Pathway CBN21B-43B-65B resulted in the most thermodynamically stable product with Gibbs free energy change of −257.5 kJ/mol. All three water molecules were eliminated from the NR-end, that is, from 21B, 43B, and 65B positions. The calculated enthalpy and entropy changes amounted to 137.7 kJ/mol and 510 J/mol K, respectively.

3.1.3. Trimer. A total of 16 reactions were investigated for the single dehydration of cellotriosan (see Supporting Information Table S6). Results show that CTN34A gives the most thermodynamic product with Gibbs free energy change equal to −82.3 kJ/mol. This pathway entails the cleavage of the hydroxyl group from carbon 3 with a concerted proton loss from carbon 4 in the LG-end. Enthalpy and entropy changes of this route accounted for 53.3 kJ/mol and 184 J/mol K, respectively.

For the double dehydration of cellotriosan, a total of 111 dehydration permutations were studied (see Supporting Information Table S7). Results reveal that CTN43C−65C showed the most thermodynamically stable product, with Gibbs free reaction energy equal to −177.8 kJ/mol. That is, removing both water molecules from the NR-end. Specifically, the hydroxyl group is lost from carbon 4 and the hydrogen from carbon 3 for the first water molecule, while for the second water molecule, the hydroxyl group and hydrogen originate from carbon 6 and carbon 5, respectively. Additionally, the enthalpy and entropy changes of the second dehydration event were calculated to be 80.0 kJ/mol and 333 J/mol K, respectively.

https://doi.org/10.1021/acs.energyfuels.3c00641
Energy Fuels 2023, 37, 7834−7847

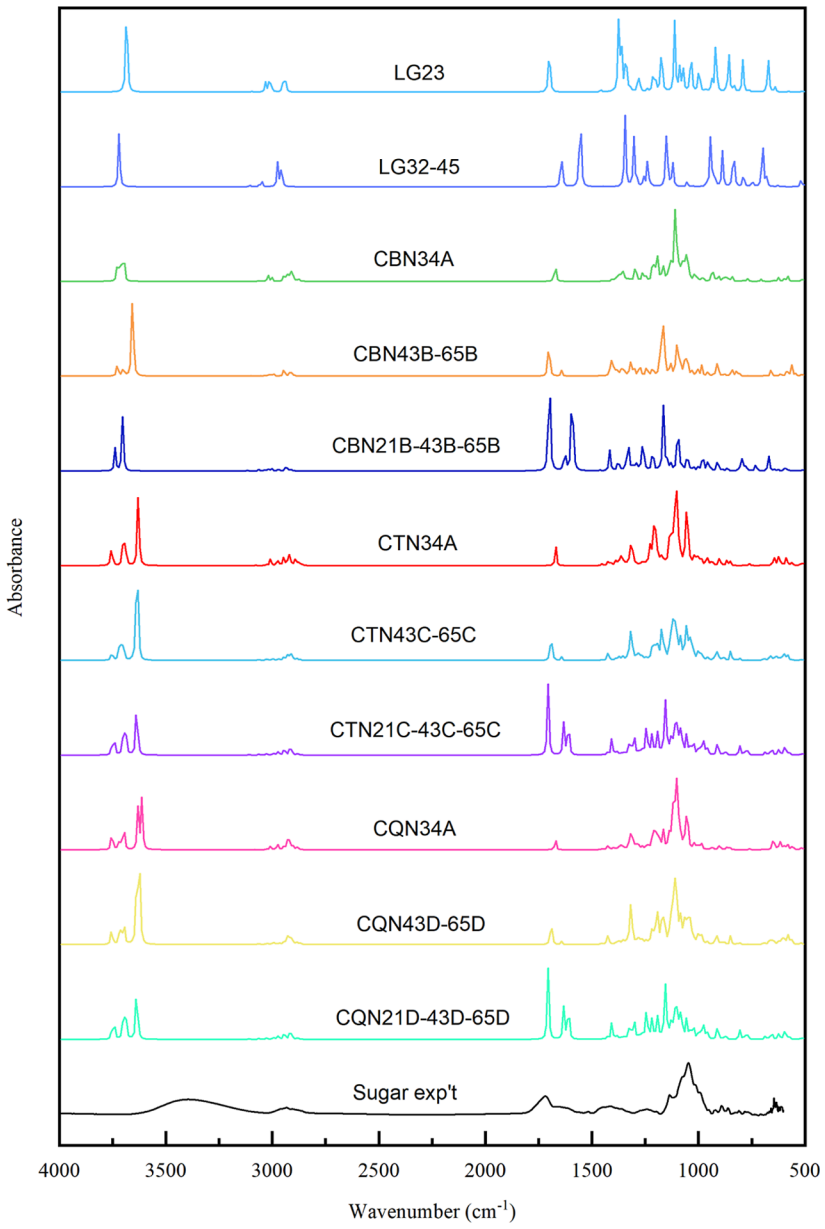

Figure 5. Theoretical FTIR spectra of the identified dehydrated anhydrosugars.

Moreover, removing three water molecules from cellotriosan resulted in the investigation of 107 reaction pathways (see Supporting Information Table S8). CTN21C−43C−65C was observed to be the most thermodynamically stable product with Gibbs free energy change of −269.8 kJ/mol. All three water molecules were lost from the NR-end, again indicating the ease of dehydration reactions at the NR-end. Enthalpy and entropy changes of this pathway correspond to 129.3 kJ/mol and 516 J/mol K, respectively.

3.1.4. Tetramer. Single dehydration of celloquatrosan resulted in a total of 21 potential dehydration pathways (see Supporting Information Table S9), revealing CQN34MacA as the most stable product with Gibbs free energy change equal to −79.1 kJ/mol. This pathway involves the removal of the hydroxyl group from carbon 3 and proton loss from carbon 4 in the LG-end. Enthalpy and entropy change of this route accounted for 53.9 kJ/mol and 172 J/mol K, respectively.

For the double dehydration of celloquatrosan, a total of 66 reaction pathways (see Supporting Information Table S10) were investigated. Reaction pathways which are expected to yield less stable products as evidenced in the dimers and trimers were not considered in this calculation. The CQN43D-65D pathway was found to be the most stable route with a Gibbs free energy of −164.5 kJ/mol. Both water molecules were desorbed from the NR-end. The enthalpy and entropy changes were correspondingly 93.5 kJ/mol and 334 J/mol K.

Finally, a total of 69 reaction pathways were studied for the triple dehydration of celloquatrosan (see Supporting Information Table S11), resulting in CQN21D-43D-65D being the most thermodynamically stable product with a Gibbs free energy change of −255.0 kJ/mol. All three water molecules were lost from the NR-end. Enthalpy and entropy changes accounted for 131.13 kJ/mol and 500 J/mol K, respectively. Similarly, the reaction pathways expected to yield less stable products were not investigated.

https://doi.org/10.1021/acs.energyfuels.3c00641
Energy Fuels 2023, 37, 7834−7847

In summary, results revealed that the LG-end is more stable than the NR-end. The thermodynamic stabilities of product molecules undergoing sequential dehydration events showed that most of the water molecules are eliminated from the NR-end, forming conjugated compounds. This result is consistent for the oligomeric units of the anhydrosugars (dimer, trimer, and tetramer) except for the single dehydration reactions exhibiting greater stability of products when water is eliminated from carbons 3 and 4 of the LG-end. According to Mamleev et al.,[5,22] dehydration reaction mostly happens at the NR-end and not from the LG-end because LG is a stable product.

3.2. Theoretical Spectra of the Dehydrated Anhydrosugars. *3.2.1. Fourier Transform Infrared.* Figure 5 shows the theoretical FTIR spectra of the proposed structures of dehydrated anhydrosugars and the experimental result of the whole sugar. A scale factor of 0.9567 was applied to the calculated vibrational frequencies toward generating the theoretical IR spectra.[34] The theoretical peaks conform to experimental results reported in previous works.[37,38] These include the hydroxyl functional group seen at 3500 to 3887 cm^{-1}, C−H vibrations from the alkane groups (2875 to 3000 cm^{-1}), alkenes and conjugated CC bond (1605 to 1750 cm^{-1}), C−C stretch from alkanes (1500 to 1550 cm^{-1}), and the C−O stretch from alcohols (1047 to 1250 cm^{-1}). The region between 1605 and 1750 cm^{-1} was shown to be more intense when more water molecules are eliminated, resulting in the formation of conjugated systems upon dehydration. The discrepancies on the OH stretches, which is observed to be broad in the experimental result, could be attributed to residual water. Nonetheless, there is a strong qualitative agreement of the FTIR results of the model compounds and the experimental analysis of the whole sugar especially in the fingerprint region. The fingerprint regions of both experimental and modeling yields are within the absorbance range of the water-soluble (WS) bio-oil fraction reported in the literature.[12]

3.2.2. Nuclear Magnetic Resonance. Figure 6 displays the theoretical ^{1}H NMR spectra of the dehydrated anhydrosugar oligomers and the experimental result of the whole sugar. Results show that the most downfield/de-shielded regions at 4.5 to 6.1 ppm are the proton types originating from alkenes and conjugated CC systems, where the dehydration reaction occurred. The spectral areas at 3.0 to 4.5 ppm are the protons attached to carbon atoms associated with the alcohol groups. Lastly, regions at 0.2 to 2.2 ppm are attributed to the protons from alkanes. The peak observed at 2.5 ppm for the experimental sugar is traced back to the DMSO solvent. Compared to the experimental ^{1}H NMR result of the whole sugar, the peaks of the proposed dehydrated sugar structures are within the range of chemical shifts. These modeling and experimental chemical shifts of the pyrolytic sugar also confirm qualitatively to the experimental results for pyrolysis bio-oils reported previously.[14]

Figure 7 shows the theoretical ^{13}C NMR spectra of the proposed structures and the experimental spectra of the whole sugar. The CC bond from 160.0 to 180.0 ppm and 100 to 120 ppm represented the alkenes and conjugated structure of the dehydrated sugars. Spectral regions between 60.0 and 100.0 ppm originated from the singly bonded carbon atoms attached to hydroxyl/alcohol groups (aliphatic C−O), with the non-ring carbon atom (carbon 6) being the most up-field. Most of the crowding is seen in this region due to the significant presence

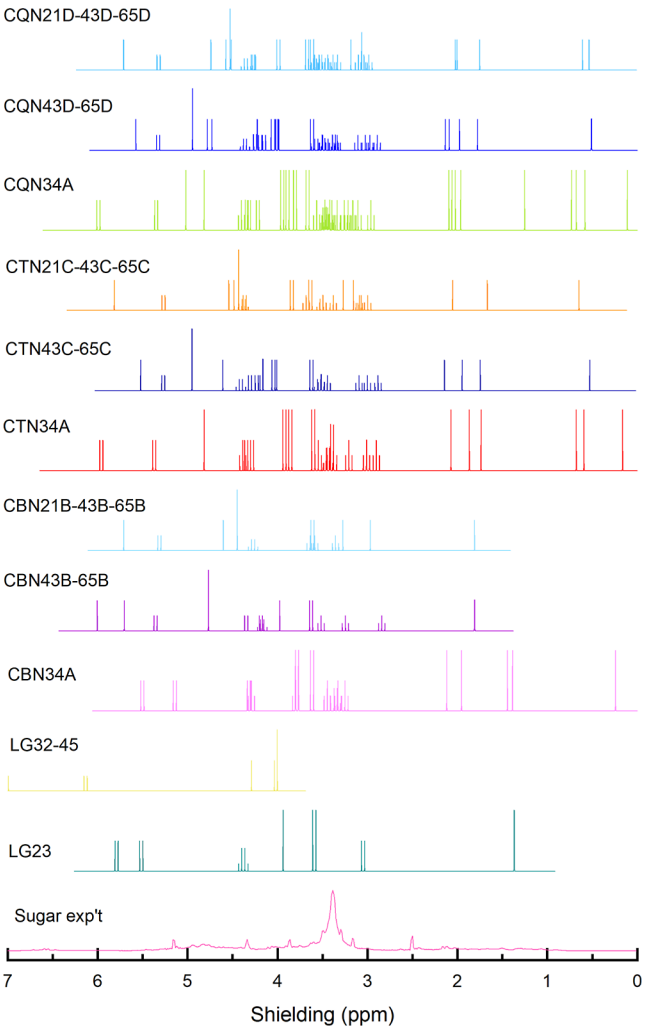

Figure 6. Theoretical ^{1}H NMR spectra of the dehydrated anhydrosugars.

of alkane and aliphatic groups. These modeling yields are in good qualitative agreement with the experimental result of the whole sugar. A ^{13}C NMR analysis on the WS bio-oil fraction from which the whole sugar was extracted (Figure 8) also shows that our modeling results are within the expected chemical shift range.[12] Though there are more peaks in the WS fraction due to the presence of phenols and other aromatic compounds, the integration region under 60.8 to 95.8 ppm of the WS fraction was reported to represent the aliphatic C−O associated with hydroxyl groups, and peaks at 95.8 to 125.0 ppm, 125.0−142.0 ppm, and 142.0 to 166.5 ppm represented aromatic C−H, aromatic C−C, and aromatic C−O, respectively.[12] The aliphatic C−O region is consistent with our modeling result. The aromatic regions in the WS fractions under 142.0 to 160.0 ppm and 170.0 to 180.0 ppm are shown to have very low intensity in our experimental ^{13}C NMR result because the phenols and aromatic compounds are no longer present in the pyrolytic sugar.

These theoretical 1-D ^{1}H and ^{13}C NMR of the sugar conforms to the experimental 2-D heteronuclear single quantum coherence spectroscopy (HSQC) NMR of bio-oil showing the presence of pyrolytic sugars as evidenced by the alcohol functional groups around 60 to 100 ppm chemical shifts for the ^{13}C NMR and 3 to 5 ppm for the ^{1}H NMR.[49]

https://doi.org/10.1021/acs.energyfuels.3c00641
Energy Fuels 2023, 37, 7834−7847

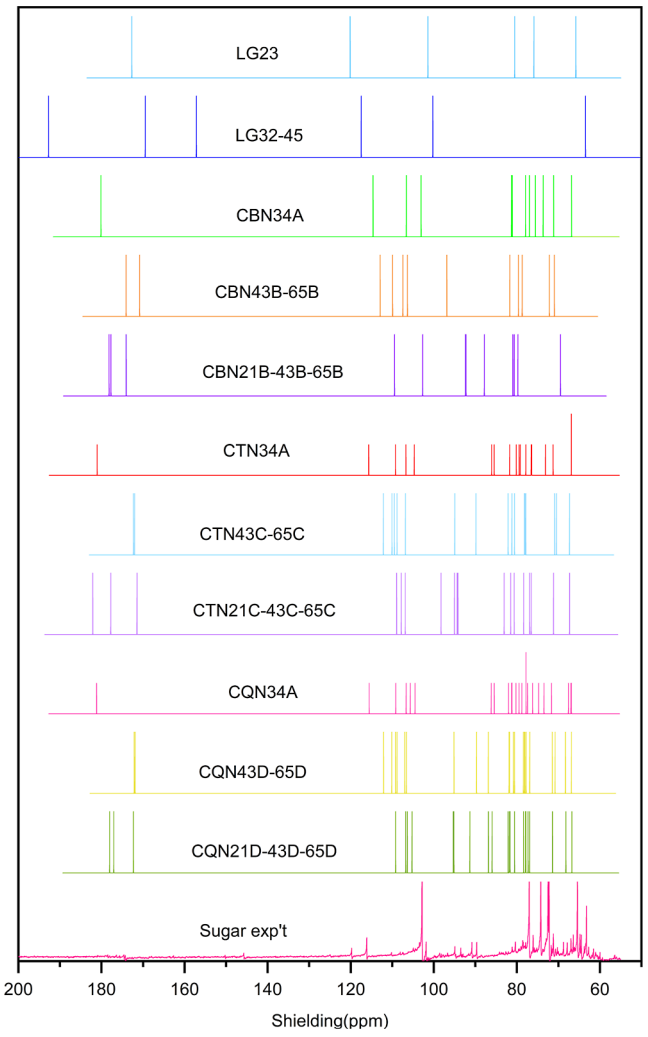

Figure 7. Theoretical ^{13}C NMR spectra of the dehydrated anhydrosugars.

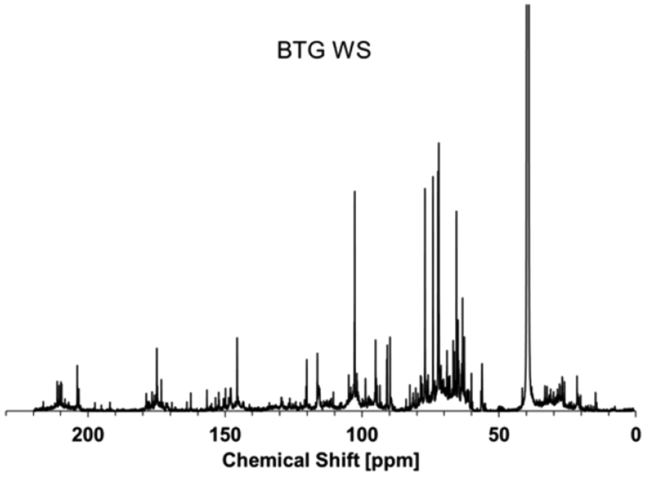

Figure 8. Experimental ^{13}C NMR spectra of the WS BTG bio-oil fraction. Reproduced with permission from Ref 12. Copyright 2023. ACS Publications.

The functional groups found in the theoretical NMR results are consistent with the functional groups identified in the FTIR results.

3.3. Thermodynamic and Physical Properties of the Proposed Oligomeric Structures.

3.3.1. Physical Properties. Table 2 shows the results for the estimated physical properties of the proposed oligomeric sugar. The dehydrated oligomeric sugars were first broken down into sets of functional groupings as proposed in the literature.[29,42,47] The physical properties investigated include critical properties like temperature, pressure, and volume, normal boiling point and melting point, and enthalpy of vaporization and fusion. These properties are fundamental parameters to predict thermodynamic behavior. The procedures used is described elsewhere.[42] There are no literature data found for comparison for the thermodynamic and physical properties of anhydrous-oligosugar molecules, as they have not been studied in the past.[14] Thus, we have used experimental data for levoglucosan and cellobiosan as the point of reference, only if available. Otherwise, the estimation of Fonts et al.[42] for levoglucosan and cellobiosan was used as point references.

For the critical temperature, the Joback[30] method gave a higher value than the Lydersen et al.'s[55] method except for the trimer which has a very high value and thus needs to be treated with caution, since these molecules are bigger than the molecules used for GCM models. Similarly, Fonts et al. estimated a high value averaging to 832.25 and 1456.1 K for the levoglucosan and cellobiosan, respectively. The more dehydrated the compound, the lower is the critical temperature. That is, the twice dehydrated cellobiosan has the lowest critical temperature. Critical temperature is the maximum possible temperature, at which the compound can exist as a liquid. Estimation of the critical pressure and critical volume resulted in quite closer values for both the Joback[30] and Lydersen et al.[55] methods. Also, these values are not too far from the estimated values reported by Fonts et al.[42] for levoglucosan (5.12 MPa, 375 cm^3/mol) and cellobiosan (3.32 MPa, 739 cm^3/mol).

For the normal boiling point, using the Joback[30] method gave a closer value to experimental results for levoglucosan, cellobiosan, and cellotriosan accounting for 658 K,[50] 853 K,[11] and 1063 K,[22] respectively. Similarly, Le de et al.[56] obtained almost the same values of 612, 854, and 1065 K for the levoglucosan, cellobiosan, and cellotriosan, respectively. Mamleev et al.[22] also reported a true boiling point of levoglucosan, which is in the range of 563 to 573 K. The estimated T_b values for the cellobiosan and cellotriosan are higher than the typical fast pyrolysis temperature (773 K). This is consistent with the experimental results reported by Pecha et al.,[23] where these molecules are driven by the ejection mechanism instead of vaporizing during the fast pyrolysis reaction. Similarly, Gong et al.[51] reported that at 773 K, there are no sugars or anhydrosugars detected during the reaction, because almost all of the cellulose have already decomposed at such high temperature. For the normal melting point, estimation using both Joback[30] and Perez-Ponce[58] methods gave quite a similar value. Oja and Suuberg[52] recorded a melting point of 453 K for levoglucosan and 513 K for cellobiose. The enthalpy of vaporization at boiling point and room temperature (298 K) resulted in a closer value for both the methods applied, except for thrice the dehydration of cellotriosan, which has values quite far from each other.

Table 3 shows estimated enthalpy of formation, standard Gibbs free energy of formation, and the heat capacity estimated under ideal gas by Joback, Harrison and Seaton, and DFT methods. Standard Gibbs free energy is a useful

https://doi.org/10.1021/acs.energyfuels.3c00641
Energy Fuels 2023, 37, 7834−7847

Table 2. Estimated Physical Property Values for Each Proposed Structure of the Anhydrosugars

	monomer		dimer			trimer			tetramer			
physical property	LG 23	LG 32-45	CBN 34A	CBN 43B-65B	CBN 21B-43B-65B	CTN 34A	CTN 43C-65C	CTN 21C-43C-65C	CQN 34A	CQN 34D-65D	CQN 21D-43D-65D	refs
critical temp. (T_c, K)	789	726	1310	1190	1101	2356	2034	1808	7420	5006	3840	30, 60
	668	611	1072	1030	1127	2794	2827	5674	−4361[b]	−3794[b]	−2001[b]	55
critical pressure, (Pc, MPa)	5.6	5.6	4.0	3.8	3.8	3.0	2.8	2.8	2.3	2.2	2.2	30, 60
	4.7	4.8	2.7	2.7	2.8	1.8	1.9	1.9	1.4	1.4	1.4	55
critical volume, (Vc, cm3/mol)	334	304	696	662	630	1057	1022	992	1418	1384	1353	30, 60
	348	312	716	678	642	1082	1046	1010	1450	1413	1373	55
normal boiling point, (Tb, K)	597	518	1061	972	894	1525	1436	1358	1989	1900	1821	30, 60
	545	496	764	725	693	979	936	904	1190	1147	1114	31
enthalpy of vaporization @ Tb, (ΔH_{vap},Tb kJ/mol)	72	57	142	125	110	211	195	180	281	264	249	30, 60
	71	47	174	167	139	75	96	115	22	34	47	57
enthalpy of vaporization, (@298.15 K) ($\Delta H_{vap,298.15K}$, kJ/mol)	106	77	250	224	192	293	301	306	304	300	295	53
	106	73	252	262	206	706	591	506	1208	1054	928	[a]
normal melting point (T_m, K)	370	331	659	616	577	949	906	867	1238	1195	1156	30, 60
	392	370	618	564	541	844	789	767	1070	1015	993	58
enthalpy of fusion, (ΔHfus,Tm, kJ/mol)	29.4	24.0	62.0	56.2	50.8	96.6	89.3	84	129	122	117	30, 60

[a]Thermodynamic equation. [b]Unreasonable.

https://doi.org/10.1021/acs.energyfuels.3c00641
Energy Fuels 2023, 37, 7834−7847

Table 3. Estimated Ideal Gas Property Values for Each Proposed Structure of the Anhydrosugars

ideal gas property	monomer		dimer			trimer			tetramer			refs
	LG 23	LG 32-45	CBN 34A	CBN 43B-65B	CBN 21B-43B-65B	CTN 34A	CTN 43C-65C	CTN 21C-43C-65C	CQN 34A	CQN 43D-65D	CQN21D-43D-65D	
gas standard enthalpy of formation (ΔH_{fG}°, kJ/mol)	−576	−337	−1448	−1191	−952	−2320	−2063	−1824	−3192	−2935	−2696	30, 60
gas standard Gibbs free energy of formation (ΔG_{fG}°, kJ/mol)	−336	−164	−894	−696	−524	−1451	−1254	−1081	−2009	−1811	−1638	30, 60
gas heat capacity at constant pressure (@298 K) ($C_{p,G}$, J/mol.K)	163	156	311	341	334	526	522	516	708	704	697	30, 60
	149	126	315	292	258	481	459	436	647	625	602	45
	132	112	315	289	272	495	470	451	674	651	631	61

parameter to determine the spontaneity of a reaction. The standard enthalpy of formation is widely used to conduct energy balances. It is the energy released or consumed during the formation of 1 mol of the substance at standard conditions. Entropy reflects the change in the degree of system disorder during the reaction.

The values estimated in this work for the singly dehydrated levoglucosan and cellobiosan for both the gas standard enthalpy and Gibbs free energy of formations are reasonable compared to the values obtained by Fonts et al. for levoglucosan ($\Delta H^{\circ}_{f,G}$ = −815.1 kJ/mol, $\Delta G^{\circ}_{f,G}$ = −508.6 kJ/mol) and cellobiosan ($\Delta H^{\circ}_{f,G}$ = −1686.3 kJ/mol, $\Delta G^{\circ}_{f,G}$ = −1065.7 kJ/mol) using the Joback method. For the gas heat capacity, results obtained from Joback, Harrison and Seaton, and the DFT methods seem to agree with each other, resulting in quite closer values. Fonts et al. reported a gas heat capacity at constant pressure equivalent to 187.2 J/mol.K for levoglucosan. This result is not too far from the estimated value for the single dehydration of levoglucosan reported in this work.

Table 4 presents the estimated condensed gas properties of the proposed structures of anhydrosugars. These properties include the liquid heat capacity, solid heat capacity, liquid standard enthalpy of formation, and the Hansen solubility parameters. Again, no literature data were found for comparison of results obtained in this study. Generally, the estimated values for the monomers and dimers seem to agree with each other for the methods applied but are seemingly far for bigger compounds like the trimer and tetramers. This may be attributed to the reason that GCM was developed and patterned for small molecules and not for the bigger ones.

For the liquid heat capacity, solid heat capacity, and liquid standard enthalpy of formation properties, Fonts et al.[42] estimated values that are close to experimental results. Hence, we can conclude that the estimated results in this work are within the range of validity of the method, considering we applied exactly the same method. Finally, Hansen solubility parameters predict the ability of one substance to dissolve into another and thus an important factor to determine suitable solvents for extraction of bio-oil compounds. The estimated Hansen solubility parameters included dispersion forces (δ_d), dipole−dipole interactions (δ_p), and hydrogen bonding (δ_{hb}).

4. CONCLUSIONS

In this work, we were able to identify and propose potential structures of the heavy oligomeric sugars obtained during cellulose pyrolysis using the DFT method and glucose-based carbohydrates as model compounds. Several potential products have been investigated, as shown in the library compiled in the Supporting Information section. It is concluded that water is typically removed from the non-reducing end. The theoretical FTIR and NMR spectra of the proposed structures of oligomeric sugars qualitatively conform to the experimental result of pyrolytic sugars. The use of QSPRs and QPPRs for the thermophysical characterization of resulting structures also shed some light on the oligomers found in bio-oil, which are fundamental for the efficient design of extraction, conversion, separation, and refining/upgrading technologies and processes. Results for the thermophysical properties cannot be compared with experimental data as they have not been studied in the past. Future efforts will help in extending this approach to the analysis of more heterogeneous feedstocks such as lignin or aggregate biomass.

https://doi.org/10.1021/acs.energyfuels.3c00641
Energy Fuels 2023, 37, 7834−7847

Table 4. Estimated Condensed Gas Property Values for Each Proposed Structure of the Anhydrosugars

	monomer		dimer			trimer			tetramer			
condensed gas property	LG23	LG 32-45	CBN 34A	CBN 43B-65B	CBN 21B-43B-65B	CTN 34A	CTN 43C-65C	CTN 21C-43C-65C	CQN 34A	CQN 43D-65D	CQN 21D-43D-65D	refs
liquid heat capacity at constant pressure, ($C_{p,l}$, J/mol K)	275	228.03	590	543	495	929	870	822	1256	1197	1149	59
solid heat capacity at constant pressure, ($C_{p,s}$, J/mol K)	180	150.96	388	359	317	596	567	539	804	775	747	46
liquid standard enthalpy of formation of individual compounds, ($\Delta H_{f,l}^{\circ}$, kJ/mol)	−682	−410	−1812	−1453	−1159	−3026	−2655	−2330	−4400	−3989	−3624	[a]
Hansen solubility parameter												54
δ_d	19.6	19.2	20.4	19.0	19.3	20.7	20.0	20.2	21.7	20.9	21.2	
δ_p	11.9	8.6	26.3	23.1	30.3	37.1	34.8	42.1	58.8	56.5	53.8	
δ_{hb}	20.4	11.7	40.8	33.1	33.6	61.2	53.7	54.2	91.1	83.7	74.8	
δ_T	30.7	24.0	52.6	44.6	49.2	74.5	67.1	71.5	110.6	103.1	94.6	

[a]Thermodynamic equation.

■ ASSOCIATED CONTENT

Supporting Information

The Supporting Information is available free of charge at https://pubs.acs.org/doi/10.1021/acs.energyfuels.3c00641.

Potential structures of the oligomeric sugars, number of atomic groups in each proposed oligomer structure, and a sample input file for the DFT calculations (PDF)

■ AUTHOR INFORMATION

Corresponding Author

Manuel Garcia-Perez − *Department of Biological Systems Engineering, Washington State University, Pullman, Washington 99164, United States;* orcid.org/0000-0002-9386-2632; Email: mgarcia-perez@wsu.edu

Authors

Melba Domes Denson − *Department of Biological Systems Engineering, Washington State University, Pullman, Washington 99164, United States; Department of Agricultural and Biosystems Engineering, Central Luzon State University, Science City of Munoz, Science City of Munoz 3120 Nueva Ecija, Philippines*

Evan Terrell − *USDA-ARS Southern Regional Research Center, New Orleans, Louisiana 70124, United States;* orcid.org/0000-0002-1079-4110

Pavlo Kostetskyy − *Department of Chemical and Biological Engineering, Northwestern University, Evanston, Illinois 60208, United States;* orcid.org/0000-0003-2796-0362

Mariefel Olarte − *Pacific Northwest National Laboratory, Richland, Washington 99352, United States;* orcid.org/0000-0003-2989-1110

Linda Broadbelt − *Department of Chemical and Biological Engineering, Northwestern University, Evanston, Illinois 60208, United States;* orcid.org/0000-0003-4253-592X

Complete contact information is available at: https://pubs.acs.org/10.1021/acs.energyfuels.3c00641

Notes

The authors declare no competing financial interest.

■ ACKNOWLEDGMENTS

Denson is very thankful to the Department of Science and Technology−Engineering Research and Development for Technology (DOST-ERDT) through Central Luzon State University, Nueva Ecija, Philippines for the financial support provided. The authors gratefully acknowledge the financial contributions received from the National Science Foundation (CBET 1926412) and the U.S. Department of Energy (DE-EE0008505). This project was also funded by the USDA/NIFA through Hatch Project WNP00701. This work was partially supported by the U.S. Department of Agriculture, Agricultural Research Service. Mention of trade names or commercial products is solely for the purpose of providing scientific information and does not imply recommendation or endorsement by USDA. USDA is an equal opportunity provider and employer.

■ REFERENCES

(1) Asif, M.; Muneer, T. Energy Supply, Its Demand and Security Issues for Developed and Emerging Economies. *Renewable Sustainable Energy Rev.* **2007**, *11*, 1388−1413.

(2) Li, X. Diversification and Localization of Energy Systems for Sustainable Development and Energy Security. *Energy Policy* **2005**, *33*, 2237−2243.
(3) Collard, F. X.; Blin, J. A Review on Pyrolysis of Biomass Constituents: Mechanisms and Composition of the Products Obtained from the Conversion of Cellulose, Hemicelluloses and Lignin. *Renewable Sustainable Energy Rev.* **2014**, *38*, 594−608.
(4) Krumm, C.; Pfaendtner, J.; Dauenhauer, P. J. Millisecond Pulsed Films Unify the Mechanisms of Cellulose Fragmentation. *Chem. Mater.* **2016**, *28*, 3108−3114.
(5) Mamleev, V.; Bourbigot, S.; Yvon, J. Kinetic Analysis of the Thermal Decomposition of Cellulose: The Main Step of Mass Loss. *J. Anal. Appl. Pyrolysis* **2007**, *80*, 151−165.
(6) Shen, D. K.; Gu, S. The Mechanism for Thermal Decomposition of Cellulose and Its Main Products. *Bioresour. Technol.* **2009**, *100*, 6496−6504.
(7) Shen, D.; Jin, W.; Hu, J.; Xiao, R.; Luo, K. An Overview on Fast Pyrolysis of the Main Constituents in Lignocellulosic Biomass to Valued-Added Chemicals: Structures, Pathways and Interactions. *Renewable Sustainable Energy Rev.* **2015**, *51*, 761−774.
(8) Shen, D.; Xiao, R.; Gu, S.; Luo, K. The Pyrolytic Behavior of Cellulose in Lignocellulosic Biomass: A Review. *RSC Adv.* **2011**, *1*, 1641−1660.
(9) Zhou, X.; Nolte, M. W.; Mayes, H. B.; Shanks, B. H.; Broadbelt, L. J. Experimental and Mechanistic Modeling of Fast Pyrolysis of Neat Glucose-Based Carbohydrates. 1. Experiments and Development of a Detailed Mechanistic Model. *Ind. Eng. Chem. Res.* **2014**, *53*, 13274−13289.
(10) Abdilla-Santes, R. M.; Agarwal, S.; Xi, X.; Heeres, H.; Deuss, P. J.; Heeres, H. J. Valorization of Humin Type Byproducts from Pyrolytic Sugar Conversions to Biobased Chemicals. *J. Anal. Appl. Pyrolysis* **2020**, *152*, 104963.
(11) Pecha, M. B.; Montoya, J. I.; Chejne, F.; Garcia-Perez, M. Effect of a Vacuum on the Fast Pyrolysis of Cellulose: Nature of Secondary Reactions in a Liquid Intermediate. *Ind. Eng. Chem. Res.* **2017**, *56*, 4288−4301.
(12) Stankovikj, F.; McDonald, A. G.; Helms, G. L.; Olarte, M. V.; Garcia-Perez, M. Characterization of the Water-Soluble Fraction of Woody Biomass Pyrolysis Oils. *Energy Fuels* **2017**, *31*, 1650−1664.
(13) Easton, M. W.; Nash, J. J.; Kenttämaa, H. I. Dehydration Pathways for Glucose and Cellobiose during Fast Pyrolysis. *J. Phys. Chem. A* **2018**, *122*, 8071−8085.
(14) Stankovikj, F.; McDonald, A. G.; Helms, G. L.; Garcia-Perez, M. Quantification of Bio-Oil Functional Groups and Evidences of the Presence of Pyrolytic Humins. *Energy Fuels* **2016**, *30*, 6505−6524.
(15) Terrell, E.; Garcia-Perez, M. Novel Strategy to Analyze Fourier Transform Ion Cyclotron Resonance Mass Spectrometry Data of Biomass Pyrolysis Oil for Oligomeric Structure Assignment. *Energy Fuels* **2020**, *34*, 8466−8481.
(16) Hu, B.; Zhang, B.; Xie, W. L.; Jiang, X. Y.; Liu, J.; Lu, Q. Recent Progress in Quantum Chemistry Modeling on the Pyrolysis Mechanisms of Lignocellulosic Biomass. *Energy Fuels* **2020**, *34*, 10384−10440.
(17) Kostetskyy, P.; Broadbelt, L. J. Progress in Modeling of Biomass Fast Pyrolysis: A Review. *Energy Fuels* **2020**, *34*, 15195−15216.
(18) Nimlos, M. R.; Blanksby, S. J.; Ellison, G.; Evans, R. J. Enhancement of 1,2-Dehydration of Alcohols by Alkali Cations and Protons: A Model for Dehydration of Carbohydrates. *J. Anal. Appl. Pyrolysis* **2003**, *66*, 3−27.
(19) Nimlos, M. R.; Blanksby, S. J.; Qian, X.; Himmel, M. E.; Johnson, D. K. Mechanisms of Glycerol Dehydration. *J. Phys. Chem. A* **2006**, *110*, 6145−6156.
(20) Hosoya, T.; Sakaki, S. Levoglucosan Formation from Crystalline Cellulose: Importance of a Hydrogen Bonding Network in the Reaction. *ChemSusChem* **2013**, *6*, 2356−2368.
(21) Zhang, X.; Yang, W.; Blasiak, W. Thermal Decomposition Mechanism of Levoglucosan during Cellulose Pyrolysis. *J. Anal. Appl. Pyrolysis* **2012**, *96*, 110−119.
(22) Mamleev, V.; Bourbigot, S.; Le Bras, M.; Yvon, J. The facts and hypotheses relating to the phenomenological model of cellulose pyrolysis. *J. Anal. Appl. Pyrolysis* **2009**, *84*, 1−17.
(23) Pecha, M. B.; Terrell, E.; Montoya, J. I.; Stankovikj, F.; Broadbelt, L. J.; Chejne, F.; Garcia-Perez, M. Effect of Pressure on Pyrolysis of Milled Wood Lignin and Acid-Washed Hybrid Poplar Wood. *Ind. Eng. Chem. Res.* **2017**, *56*, 9079−9089.
(24) Zhou, X.; Nolte, M. W.; Shanks, B. H.; Broadbelt, L. J. Experimental and Mechanistic Modeling of Fast Pyrolysis of Neat Glucose-Based Carbohydrates. 2. Validation and Evaluation of the Mechanistic Model. *Ind. Eng. Chem. Res.* **2014**, *53*, 13290.
(25) Gallo, J. M. R.; Alonso, D. M.; Mellmer, M. A.; Dumesic, J. A. Production and Upgrading of 5-Hydroxymethylfurfural Using Heterogeneous Catalysts and Biomass-Derived Solvents. *Green Chem.* **2013**, *15*, 85−90.
(26) Westerhof, R. J. M.; Oudenhoven, S. R. G.; Marathe, P. S.; Engelen, M.; Garcia-Perez, M.; Wang, Z.; Kersten, S. R. A. The Interplay between Chemistry and Heat/Mass Transfer during the Fast Pyrolysis of Cellulose. *React. Chem. Eng.* **2016**, *1*, 555−566.
(27) Constantinou, L.; Gani, R. New Group Contribution Method for Estimating Properties of Pure Compounds. *AIChE J.* **1994**, *40*, 1697−1710.
(28) Kolska, Z.; Zabransky, M.; Randov, A. Group Contribution Methods for Estimation of Selected Physico-Chemical Properties of Organic Compounds. *Thermodynamics - Fundamentals and Its Application in Science*, IntechOpen London 2012, 10.5772/49998.
(29) Gani, R. Group Contribution-Based Property Estimation Methods: Advances and Perspectives. *Curr. Opin. Chem. Eng.* **2019**, *23*, 184−196.
(30) Joback, K. G. A Unified Approach to Physical Property Estimation Using Multivariate Statistical Techniques. 1984. http://dspace.mit.edu/handle/1721.1/15374. Accessed on October 13, 2021.
(31) Stein, S. E.; Brown, R. L. Estimation of Normal Boiling Points from Group Contributions. *J. Chem. Inf. Comput. Sci.* **2002**, *34*, 581−587.
(32) Mayes, H. B.; Broadbelt, L. J. Unraveling the Reactions That Unravel Cellulose. *J. Phys. Chem. A* **2012**, *116*, 7098−7106.
(33) Patwardhan, P. R.; Brown, R. C.; Shanks, B. H. Understanding the Fast Pyrolysis of Lignin. *ChemSusChem* **2011**, *4*, 1629.
(34) Ünal, Y.; Nassif, W.; Özaydin, B. C.; Sayin, K. Scale Factor Database for the Vibration Frequencies Calculated in M06-2X, One of the DFT Methods. *Vib. Spectrosc.* **2021**, *112*, 103189−103196.
(35) Taylor, C. J.; Nix, M. G. D.; Dessent, C. E. H. Noncovalent Interactions in the Gas-Phase Conformers of Anionic Iduronate (methyl 2-O-sulfo-α-L-iduronate): Variation of Subconformer versus Ring Conformer Energetics for a Prototypical Anionic Monosaccharide Studied Using Computational Methods. *J. Phys. Chem. A* **2010**, *114*, 11153−11160.
(36) Zhao, Y.; Truhlar, D. G. The M06 suite of density functionals for main group thermochemistry, thermochemical kinetics, noncovalent interactions, excited states, and transition elements: two new functionals and systematic testing of four M06-class functionals and 12 other functionals. *Theor. Chem. Acc.* **2008**, *120*, 215−241.
(37) Han, Y.; Paiva Pinheiro Pires, A.; Denson, M.; McDonald, A. G.; Garcia-Perez, M. Ternary Phase Diagram of Water/Bio-Oil/Organic Solvent for Bio-Oil Fractionation. *Energy Fuels* **2020**, *34*, 16250−16264.
(38) Stankovikj, F.; Garcia-Perez, M. TG-FTIR Method for the Characterization of Bio-Oils in Chemical Families. *Energy Fuels* **2017**, *31*, 1689−1701.
(39) Nimlos, M. R.; Evans, R. J. Levoglucosan Pyrolysis. *Fuel Chem. Div. Prepr.* **2002**, *47*, 393.
(40) Zhou, S.; Garcia-Perez, M.; Pecha, B.; Kersten, S. R. A.; McDonald, A. G.; Westerhof, R. J. M. Effect of the Fast Pyrolysis Temperature on the Primary and Secondary Products of Lignin. *Energy Fuels* **2013**, *27*, 5867−5877.
(41) Stanford, J. P.; Hall, P. H.; Rover, M. R.; Smith, R. G.; Brown, R. C. Separation of Sugars and Phenolics from the Heavy Fraction of

https://doi.org/10.1021/acs.energyfuels.3c00641
Energy Fuels 2023, 37, 7834−7847

Bio-Oil Using Polymeric Resin Adsorbents. *Sep. Purif. Technol.* **2018**, *194*, 170−180.
(42) Fonts, I.; Atienza-Martínez, M.; Carstensen, H. H.; Benés, M.; Pinheiro Pires, A. P.; Garcia-Perez, M.; Bilbao, R. Thermodynamic and Physical Property Estimation of Compounds Derived from the Fast Pyrolysis of Lignocellulosic Materials. *Energy Fuels* **2021**, *35*, 17114−17137.
(43) Marrero, J.; Gani, R. Group-Contribution Based Estimation of Pure Component Properties. *Fluid Phase Equilib.* **2001**, *183*−*184*, 183−208.
(44) Manrique, R.; Terrell, E.; Kostetskyy, P.; Chejne, F.; Olarte, M.; Broadbelt, L.; García-Pérez, M. Elucidating Biomass-Derived Pyrolytic Lignin Structures from Demethylation Reactions through Density Functional Theory Calculations. *Energy Fuels* **2023**, *37* (7), 5189−5205.
(45) Harrison, B. K.; Seaton, W. H. Solution to Missing Group Problem for Estimation of Ideal Gas Heat Capacities. *Ind. Eng. Chem. Res.* **1988**, *27*, 1536−1540.
(46) Hurst, J. E.; Keith Harrison, B. Estimation of Liquid and Solid Heat Capacities Using a Modified Kopp's Rule. *Chem. Eng. Commun.* **1992**, *112*, 21−30.
(47) Stefanis, E.; Panayiotou, C. Prediction of Hansen Solubility Parameters with a New Group-Contribution Method. *Int. J. Thermophys.* **2008**, *29*, 568−585.
(48) Teixeira, A. R.; Mooney, K. G.; Kruger, J. S.; Williams, C. L.; Suszynski, W. J.; Schmidt, L. D.; Schmidt, D. P.; Dauenhauer, P. J. Aerosol Generation by Reactive Boiling Ejection of Molten Cellulose. *Energy Environ. Sci.* **2011**, *4*, 4306−4321.
(49) Yu, Y.; Chua, Y. W.; Wu, H. Characterization of Pyrolytic Sugars in Bio-Oil Produced from Biomass Fast Pyrolysis. *Energy Fuels* **2016**, *30*, 4145−4149.
(50) Shoji, T.; Kawamoto, H.; Saka, S. Boiling Point of Levoglucosan and Devolatilization Temperatures in Cellulose Pyrolysis Measured at Different Heating Area Temperatures. *J. Anal. Appl. Pyrolysis* **2014**, *109*, 185−195.
(51) Gong, X.; Yu, Y.; Gao, X.; Qiao, Y.; Xu, M.; Wu, H. Formation of Anhydro-Sugars in the Primary Volatiles and Solid Residues from Cellulose Fast Pyrolysis in a Wire-Mesh Reactor. *Energy Fuels* **2014**, *28*, 5204.
(52) Oja, V.; Suuberg, E. M. Vapor Pressures and Enthalpies of Sublimation of D-Glucose, D-Xylose, Cellobiose, and Levoglucosan. *J. Chem. Eng. Data* **1999**, *44*, 26−29.
(53) Watson, K. M. Thermodynamics of the Liquid State. *Ind. Eng. Chem.* **1943**, *35*, 398−406.
(54) Hansen, C. M. *Hansen Solubility Parameters Second Edition: A User's Handbook*; CRC Press: Boca Raton, FL, 2007, pp 10−11. 347, 423.
(55) Lydersen, A. L.; Greenkorn, R. A.; Hougen, O. A. *Estimation of Critical Properties of Organic Compounds Engineering Experiment Station Report 3*; College of Engineering, University of Wisconsin: Madison, WI, 1955; pp 1−22.
(56) Le de, J., Diebold, J. P., Peacocke, G. V. C., Piskorz, J. Bridgwater, A. V., Eds., *Fast Pyrolysis of Biomass: A Handbook*, CPL Press, Newbury, 1999, pp. 51−65
(57) Riedel, L. Eine neue universelle Dampfdruckformel Untersuchungen über eine Erweiterung des Theorems der übereinstimmenden Zustände. Teil I. *Chem. Ing. Tech.* **1954**, *26*, 83−89.
(58) Pérez Ponce, A. A.; Salfate, I.; Pulgar-Villarroel, G.; PalmaChilla, L.; Lazzus, J. A. New group contribution method for the´ prediction of normal melting points. *J. Eng. Thermophys.* **2013**, *22*, 226−235.
(59) Chueh, C. F.; Swanson, A. C. Estimation of liquid heat capacity: Estimation of liquid heat capacity. *J. Chem. Eng.* **1973**, *51*, 596−600.
(60) Joback, K. G.; Reid, R. C. Estimation of pure-component properties from group-contributions. *Chem. Eng. Commun.* **1987**, *57*, 233−243.
(61) Frisch, M. J., Trucks, G. W., Schlegel, H. B., Scuseria, G. E., Robb, M. A., Cheeseman, J. R., Scalmani, G., Barone, V., Petersson, G. A., Nakatsuji, H., Li, X., Caricato, M., Marenich, A. V., Bloino, J., Janesko, B. G., Gomperts, R., Mennucci, B., Hratchian, H. P., Ortiz, J. V., Izmaylov, A. F., Sonnenberg, J. L., Williams-Young, D., Ding, F., Lipparini, F., Egidi, F., Goings, J., Peng, B., Petrone, A., Henderson, T., Ranasinghe, D., Zakrzewski, V. G., Gao, J., Rega, N., Zheng, G., Liang, W., Hada, M., Ehara, M., Toyota, K., Fukuda, R., Hasegawa, J., Ishida, M., Nakajima, T., Honda, Y., Kitao, O., Nakai, H., Vreven, T., Throssell, K., Montgomery, J. A., Jr., Peralta, J. E., Ogliaro, F., Bearpark, M. J., Heyd, J. J., Brothers, E. N., Kudin, K. N., Staroverov, V. N., Keith, T. A., Kobayashi, R., Normand, J., Raghavachari, K., Rendell, A. P., Burant, J. C., Iyengar, S. S., Tomasi, J., Cossi, M., Millam, J. M., Klene, M., Adamo, C., Cammi, R., Ochterski, J. W., Martin, R. L., Morokuma, K., Farkas, O., Foresman, J. B., Fox, D. J., *Gaussian 16*, Revision C.01, Gaussian, Inc., Wallingford CT, 2019

https://doi.org/10.1021/acs.energyfuels.3c00641
Energy Fuels 2023, 37, 7834−7847